UTU Publishing Group

Bulletin of Biomedical Science

Journal Homepage: www.utu.com.sg

ARTICLE

MiR-139-5p reduces reactive oxygen species levels in hepatic stellate cells and alleviates the progression of hepatic fibrosis by targeting SMOX

Na Cheng[1*], Songsong Yuan[1*], Chuang Nie[1], Wenfeng Zhang[1], Xiuhua Kang[2], Tianxin Xiang[1]

[1]Jiangxi Medical Center for Critical Public Health Events, The First Affiliated Hospital, Jiangxi Medical College, Nanchang University, Nanchang, Jiangxi 330052, P.R. China
[2]Department of Hospital Infection Control, The First Affiliated Hospital, Jiangxi Medical College, Nanchang University, Nanchang, Jiangxi 330006, P.R. China
[*]Na Cheng and Songsong Yuan have contributed equally to this work

ARTICLE INFO

Received 12 February 2024
Accepted 2 March 2024
Online 28 April 2024

KEY WORDS:
Hepatic fibrosis;
MiR-139-5p;
SMOX;
ROS;
Hepatic stellate cells

Abstract

Objective This study aims to investigate the roles and the molecular mechanisms of miR-139-5p and SMOX in hepatic fibrosis (HF). **Methods** Relative levels of miR-139-5p and SMOX in in vitro and in vivo HF models were determined by RT-qPCR, Western blot, and immunohistochemical staining. Activation of the hepatic stellate cell (HSC) line HSC-T6 was achieved by lipopolysaccharide (LPS) induction. Subsequently, the regulatory effects of miR-139-5p and SMOX on HSC-T6 cell behaviors were examined. The targeting relationship between miR-139-5p and SMOX was ascertained by dual-luciferase reporter assay. **Results** Downregulated miR-139-5p and upregulated SMOX were examined in rat fibrotic liver tissues. MiR-139-5p significantly inhibited LPS-induced activation of HSC-T6 cells, reduced reactive oxygen species (ROS) levels, and inhibited cell viability. SMOX is the direct target of miR-139-5p, and is capable of reversing the protective effect of miR-139-5p, which halts the progression of HF. **Conclusions** MiR-139-5p is significantly downregulated in the progression of HF, which subsequently halts the progression of HF by targeting and downregulating SMOX. Thus, miR-139-5p can serve as a potential biomarker and therapeutic target of HF.

Introduction

Chronic liver disease is a severe health issue worldwide. It is estimated that globally, chronic liver disease affects hundreds of millions of people (Xiao et al., 2019). Hepatic fibrosis (HF) is an important link in the progression of chronic liver disease, which can deteriorate into cirrhosis and even liver cancer (Coulouarn & Clement, 2014). At present, liver

Corresponding author: Tianxin Xiang, Jiangxi Medical Center for Critical Public Health Events, The First Affiliated Hospital, Jiangxi Medical College, Nanchang University, Nanchang, Jiangxi 330052, P.R. China. txxiangmed@163.com.

transplantation is the only method for curing decompensated cirrhosis. However, its application is extremely limited due to shortages of donated organs and the high medical cost (Jesudian et al., 2016). HF is usually caused by the imbalanced production and degradation of the extracellular matrix (ECM), consisting mainly of collagens in hepatic stellate cells (HSCs) (Hernandez-Gea & Friedman, 2011). They are the main source of excessively deposited ECM during the progression of HF. In patients with chronic liver injuries, a long-term persistent inflammatory response and oxidative stress activates HSCs and promotes their transformation to myofibroblast-like cells. As a result, abundant α-SMA, collagens, and elastin are produced and accumulate, leading to the development of HF (Tsai, Lin, & Huang, 2010).

Spermine oxidase (SMOX) is a flavin adenine dinucleotide (FAD)-dependent oxidase involved in polyamine metabolism. Through the formation of homodimers, SMOX directly catalyzes spermine to produce spermidine and a large amount of hydrogen peroxide as the byproduct (Cervelli, Amendola, Polticelli, & Mariottini, 2012; Leonetti et al., 2017). SMOX is closely linked with inflammatory response and several types of tumors (Murray-Stewart et al., 2016). Recent studies have found that SMOX is upregulated in chronic hepatitis and hepatocellular carcinoma cases. SMOX is positively correlated with the severity of clinical symptoms of hepatocellular carcinoma, suggesting that SMOX may promote the development of HF (Hu et al., 2018).

MicroRNAs (miRNAs) are short non-coding RNAs containing 22-23 nucleotides, and they participate in various biological functions by regulating post-transcription and gene functions (Jie et al., 2021). Typically, a single-stranded RNA serves as a mature miRNA that forms RNA-induced silencing complex (RISC) alongside the Argonaute protein. RISC further induces degradation or translation inhibition of downstream targets by binding to their 3'-untranslated region (3'-UTR) (Suzuki, Katsura, Matsuyama, & Miyazono, 2015). MiR-605 is a newly discovered miRNA, and its function in HF is currently unclear.

In the present study, miR-139-5p was found to alleviate the progression of HF by directly targeting SMOX. Therefore, we speculated that miR-139-5p targeted SMOX and inhibited its transcription, thus arresting the development of HF by decreasing reactive oxygen species (ROS) levels, downregulating α-SMA and TGF-β in HSCs, and reducing the massive production and deposition of the ECM.

Methods and Materials

1. Creating an HF rat model in vivo

A total of 12 male Sprague-Dawley (SD) rats weighing 200 ± 20 g (Guangdong Medical Laboratory Animal Center) were randomly assigned to the control group or the HF group, with 6 rats in each group. HF was induced by subcutaneous injection of 0.3 ml/100 g CCl_4 three times a week for 8 weeks. Rats in the control group were subcutaneously injected with isodose saline. Rats were euthanized, and then, their liver tissues were harvested.

2. H&E staining

Rat liver tissues fixed in 4% paraformaldehyde were prepared for tissue sections by embedding in paraffin, immersing the paraffin sections in xylene twice for 20 min each time, in anhydrous ethanol twice for 5 min each time, in 75% ethanol for 5 min, and then finally washing in ddH_2O. A hematoxylin-eosin (HE) staining kit (Sangon Biotech, Shanghai, China, catalog number: E607318) was used in the present study. Briefly, sections were stained with hematoxylin for 5 min. After differentiation and bluing, the sections were washed in ddH_2O, sequentially dehydrated in 85% and 5% ethanol, and stained with eosin for 5 min. After incubation three times in anhydrous ethanol, and twice in xylene, the sections were mounted using neutral gum for observation under a microscope.

3. Cell culture

The rat HSC cell line HSC-T6 (Procell, Wuhan, China, catalog number: CL-0116) was cultivated in Dulbecco's modified Eagle's medium (DMEM, Procell, Wuhan, China, catalog number: 164210-500) containing 10% fetal bovine serum (FBS, Procell, Wuhan, China, catalog number: PM150210) and 1% penicillin and streptomycin in a humidified incubator containing 5% CO_2 and 95% air at 37°C. Cryopreservation using DMEM containing 40% FBS, 10% dimethyl sulfoxide (DMSO), and 55% glucose was performed until the cells were grown to higher than 80% confluence by trypsin digestion.

4. Cell transfection

MiR-139-5p mimics, miR-139-5p inhibitor, and their negative controls, mimic-NC and inhibitor-NC, were provided by RiboBio Co., Ltd. (Guangzhou, China). Lipofectamine® 2000 transfection reagent (Invitrogen; Thermo Fisher Scientific, Inc.) was used in cell transfection. Briefly, cells were seeded in a 12-well plate (1×10^5 cells per well) and cultured to 80% confluence. After 4-h starvation in serum-free DMEM, 100 nM transfection mixture containing the plasmid and Lipofectamine® 2000 reagent was added for 40-min incubation. Fresh medium was replaced at 24 h, and transfection efficacy was examined by RT-qPCR.

5. 3-(4,5-Dimethylazol-2-yl)-2,5-diphenyltetrazolium bromide (MTT) assay

HSC-T6 cells were seeded in a 96-well plate with 5×10^3 cells/well cultivated in 200 μL of DMEM containing 10%

FBS, and 1% penicillin and streptomycin. Briefly, 15 μl of MTT solution (15 mg/ml, Sangon Biotech, Shanghai, China, catalog number: A600799) was added at 6, 12, 18, 24, 30, and 36 h, respectively. After cell culture for 4 h at 37°C, cells in each well were lysed in 150 μL of DMSO for 10 min at room temperature, and the optical density at 490 nm was measured using an HBS-1101 microplate reader (DeTie, China).

6. RT-qPCR

Total RNA in HSC-T6 cells or liver tissues was isolated using TRIzol reagent (Invitrogen, USA), and 1 μg total RNA was reversely transcribed to cDNA using the Takara Primescript™ RT reagent kit. Subsequently, qPCR was performed using a SYBR Premix Ex Taq™II with Tli RNaseH (Takara Bio, Inc.) using an ABI Prism 7500 system (Thermo Fisher Scientific, Inc.). Relative levels were calculated using the $2^{-\Delta\Delta CT}$ method with glyceraldehyde-3-phosphate dehydrogenase (GAPDH) or U6 as the internal reference. The primer sequences are listed in Table 1.

7. Western blot

Total proteins in HSC-T6 cells or liver tissues were isolated using radioimmunoprecipitation (RIPA) buffer (Beyotime Institute of Biotechnology, China) containing phenylmethylsulfonyl fluoride (PMSF) and protease inhibitor. Protein concentrations were measured using a bicinchoninic acid (BCA) protein assay kit (Beyotime Institute of Biotechnology, China). Protein samples (50 μg) were loaded on sodium dodecyl sulfate-polyacrylamide gel electrophoresis (SDS-PAGE) gels, electrophoresed, and subsequently transferred to polyvinylidene difluoride (PVDF) membranes at 300 mA. Non-specific antigens on PVDF membranes were blocked by immersing in Tris-buffered saline (TBS) containing 0.1% Tween-20 (TBST) and 5% skim milk. After immunoblotting with primary antibodies (1:1000) at 4°C overnight and secondary antibodies (1:1000) at room temperature for 1 h, band exposure was performed using the Bio-Rad Universal Hood II Gel Doc Imaging system, and grey values were analyzed using ImageJ 1.8.0.112 software (U.S. National Institutes of Health, Bethesda, MD, USA). The antibodies were purchased from Abclonal (Abclonal, Wuhan, China), and the catalog numbers were as listed: SMOX (A11677); α-SMA (A2319); TGF-β (A18692); GAPDH (A19056); and the secondary antibody was HRP Goat Anti-Rabbit IgG (H+L) (AS014).

Table 1. Primers used in this study

Gene	Primes (5'→3')
Rno-miR-139-5p-F	TCTACAGTGCACGTGTCTCCAG
SMOX-F	CGGGGAAAATGGAAACGTCAG
SMOX-R	ACTTTGCATACCGTCCGTACT
α-SMA-F	CAGCTATTGCCGTTCCAATTGA
α-SMA-R	CCAGGGCTTCATCATTGCA
TGF-β-F	CGAGCTCGGTGGAAGGTCTCATTTTATTG
TGF-β-R	CCCAAGCTTGGGATGTAAAAGACAAACAATG
GAPDH-F	GGCACAGTCAAGGCTGAGAATG
GAPDH-R	ATGGTGGTGAAGACGCCAGTA
U6-F	ACGCAAATTCGTGAAGCGTT

8. Masson staining

Rat liver tissues were dewaxed and dehydrated in xylene and ethanol with gradient concentrations (100%, 85%, 75%, and 30%). After nuclei staining using Weigert's iron hematoxylin solution for 5-10 min, and washing in flowing water, sections were later counterstained with Ponceau S and acid fuchsin for 5-10 min. Following washing in 2% acetic acid aqueous solution, differentiation in 1% phosphomolybdic acid solution for 3-5 min, staining in aniline blue WS for 5 min, and washing in 0.2% acetic acid aqueous solution, sections were washed in 95% ethanol and anhydrous ethanol. Sections were permeabilized using xylene, mounted using neutral gum and observed under a microscope.

9. Immunohistochemical staining

Rat liver sections were incubated in xylene 3 times for 15 min each time, dehydrated in anhydrous ethanol twice for 5 min each time, 85% ethanol for 5 min, and 75% ethanol for 5 min. After washing in ddH_2O, sections were immersed in citrate buffer (pH 6.0, Sangon Biotech, Shanghai, China, catalog number: E673000) for 15-min for antigen retrieval. They were then incubated in 3% H_2O_2 in the dark for 25 min, and blocked in 3% BSA (Sangon Biotech, Shanghai, China, catalog number: E661003) at 37°C for 30 min. Incubation of primary antibodies was performed at 4°C overnight, and then, sections were washed in phosphate-buffered saline (PBS, pH 7.4) for 5 min for 3 times, and incubated with horseradish peroxidase (HRP)-labeled secondary antibodies at room temperature for 2 h. Later, sections were counterstained with diaminobenzidine (DAB) and hematoxylin for 3 min. After dehydration in ddH_2O, 75% ethanol for 5 min, 85% ethanol for 5 min, anhydrous ethanol for 5 min twice, and n-butanol for 5 min, and permeabilization in xylene for 5 min, sections were mounted using neutral gum. Positive staining of cells was observed under a microscope (XSP-8CA, Shanghai Optical Instrument Co., Ltd.).

10. Dual-luciferase reporter assay

The wild-type plasmid pGL3-SMOX-WT was constructed by amplifying complementary sequences in the SMOX 3'-UTR and promoter region of miR-139-5p and cloning them into the pGL3 3'-UTR (Genechem Inc., Shanghai, China). The

mutant-type plasmid pGL3-SMOX-Mut was constructed using a site-directed mutagenesis kit (Sangon Biotech, Shanghai, China, catalog number: B639281). Wild-type and mutant-type plasmids were co-transfected into cells with miR-139-5p mimics or mimics-NC for 48 h. Relative firefly and Renilla luciferase activities were measured using the Dual-Luciferase Reporter Gene Assay Kit (Promega, Madison, WI, USA).

11. Lentivirus infection

Overexpression lentivirus plasmid GV367-SMOX (GeneChem Inc., Shanghai, China) was generated by cleavage of GV367 plasmid using AgeI/NheI, and GV367 was used as a blank control. Lentivirus packaging was performed using a second-generation lentivirus packaging kit (GeneChem, Shanghai, China). The lentiviral plasmid, packaging vector, and envelope vector were mixed at a 4:3:2 ratio for a total DNA mass of 20 μg, and were then incubated with 1 ml of Lenti-Easy Packaging Mix (Shanghai GeneChem Co., Ltd.) for 15 min. The mixture was then incubated for another 20 min in Lipofectamine® 2000, and inoculated into 293T cell culture medium for 6 h at 37°C. 293T cells were seeded in a 12-well plate at a density of 2.5×10^5 cells/well and cultured to 80% confluence. After incubation in serum-free DMEM for 4 h, cells were transfected with lentiviruses for 3 days, as described above. Transfected cells were filtered using a 0.45-μM mesh, and were then concentrated at 70,000 × g and 4°C for 2 h. The supernatant was collected to measure the viral titers. HSC-T6 cells grown to over 80% confluence were cultured with diluted lentiviruses, and GFP-labeled cells with lentivirus transfection rate > 80% at 72 h were collected. The transfection efficacy of SMOX was finally verified by RT-qPCR.

12. Measurement of ROS levels

HSC-T6 cells were seeded in a 24-well plate and cultured to 80% confluence or higher. Next, 10 μmol/L dichlorodihydro-fluorescein diacetate (DCFH-DA) was added, and the plates were incubated at 37°C for 30 min. Green fluorescence signals in 5 randomly selected fields per well were observed under a fluorescence microscope (magnification = 100 ×). ROS levels were measured by calculating the mean fluorescent intensity (MFI).

13. Measurement of the activity of SMOX

Broken cells was mixed with 5 μmol luminol and 20 μg HRP in 100 mM glycine buffer, and incubated at 37°C for 2 min. Using the dual-sampler system, cell lysate and prepared SMOX mixture were each examined by a Promega GloMax microplate reader, and added spermine, then followed by measurement of the cumulative intensity of chemiluminescence for 20 s. The results are compared with the standard curve of H_2O_2 to obtain the active oxygen level.

14. Statistical processing

The data are expressed as the mean ± standard deviation (SD) from 3 replicates and were processed by GraphPad Prism 8.0 software. Differences between groups were compared by Student's t-test. A significant difference was determined at $p < 0.05$.

Results

1. Establishment of rat HF model and HF cell model

The HF model in rats was established by subcutaneous injection of CCl_4, followed by collection of rat liver tissues for H&E and Masson staining. In the HF group, images of stained rat liver tissues revealed fibrosis surrounding the portal area, obvious fibrous septa, and disarranged lobular structure, indicating the successful establishment of the HF model (Figure 1A, 1B). Immunohistochemical staining showed increased positive expression of α-SMA in liver tissues of HF rats (Figure 1C). Rat liver tissues were collected for extracting total RNA and proteins. As expected, we detected significantly upregulated α-SMA in the liver tissues of HF rats (Figure 1D, 1E). The results suggested that the rat liver fibrosis model was established successfully. In lipopolysaccharide (LPS)-induced HSC-T6 cells, significantly upregulated α-SMA confirmed the activation of HSCs (Figure 1F, 1G).

2. SMOX is upregulated HF model and miR-139-5p directly targets SMOX

We detected the expression level of SMOX in rat and cellular HF model. The results of RT-qPCR, western blot and immunohistochemical staining showed that the mRNA and protein levels of SMOX were significantly increased in the HF rats (Figure 2A-2C); The expression level of SMOX in cellular HF model was also significantly increased (Figure 2D, 2E). There were three fragments of the miR-139-5p promoter region that were complementarily paired with SMOX 3'-UTR, as predicted using Targetscan 7.2 (Figure 2F). As shown by dual-luciferase reporter assay, co-transfection of miR-139-5p mimics and pGL3-SMOX-WT decreased the luciferase activity by 41%. However, miR-139-5p did not influence the luciferase activity in pGL3-SMOX-MuT, confirming the targeting relationship between miR-139-5p and SMOX (Figure 2G). The results showed that SMOX is upregulated HF model and miR-139-5p directly targets SMOX.

3. MiR-139-5p weakens SMOX expression and its ability to degrade spermine

We detected the expression level of Rno-miR-139-5p, suggesting that it was significantly down regulated in both rat model and cell model (Figure 3A, 3B). The transfection efficiency of rno-miR-139-5p mimics or mimic-NC was detected (Figure 3C), and the transfection of mimics and the negative control suggested that rno-miR-139-5p could

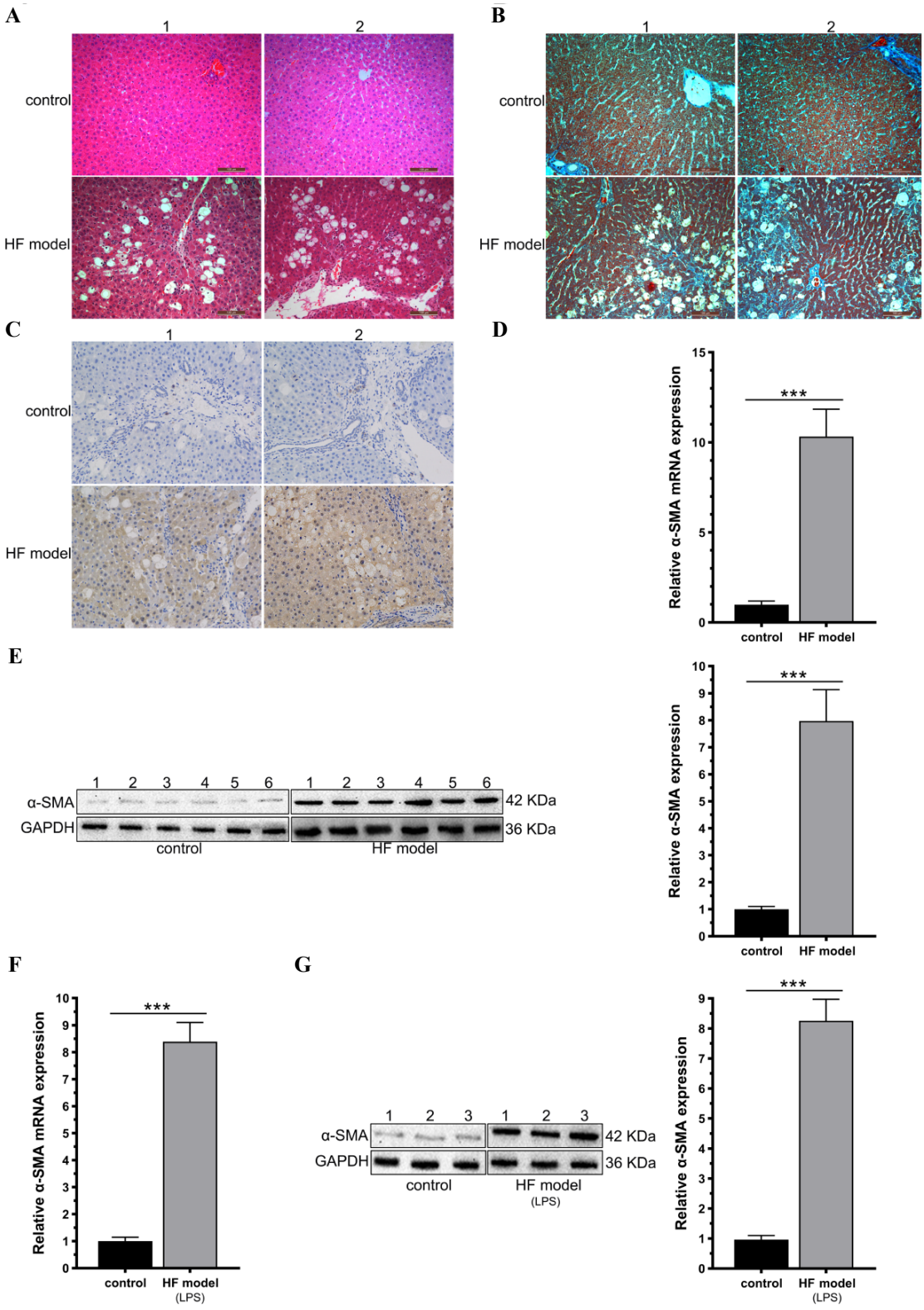

Figure 1. Establishment of rat HF model and cellular HF model

Notes: (A) HE staining of rats HF model; (B) Masson staining of rats HF model; (C) α-SMA immunohistochemical staining of rats HF model; (D) RT-qPCR detection of α-SMA expression in rats HF model; (E) Western blot detection of α-SMA expression in rats HF model; (F) RT-qPCR detection of α-SMA expression in cellular HF model; (G) Western blot detection of α-SMA expression in cellular HF model. ***: $P < 0.001$.

significantly down regulate the mRNA and protein levels of SMOX (Figure 3D, 3E). In addition, overexpression of miR-139-5p significantly decreased the ability of HSC-T6 cells to degrade spermine (Figure 3F). As demonstrated by the above findings, miR-139-5p targeted SMOX, and thus downregulated the mRNA and protein levels and the enzymatic activity of SMOX.

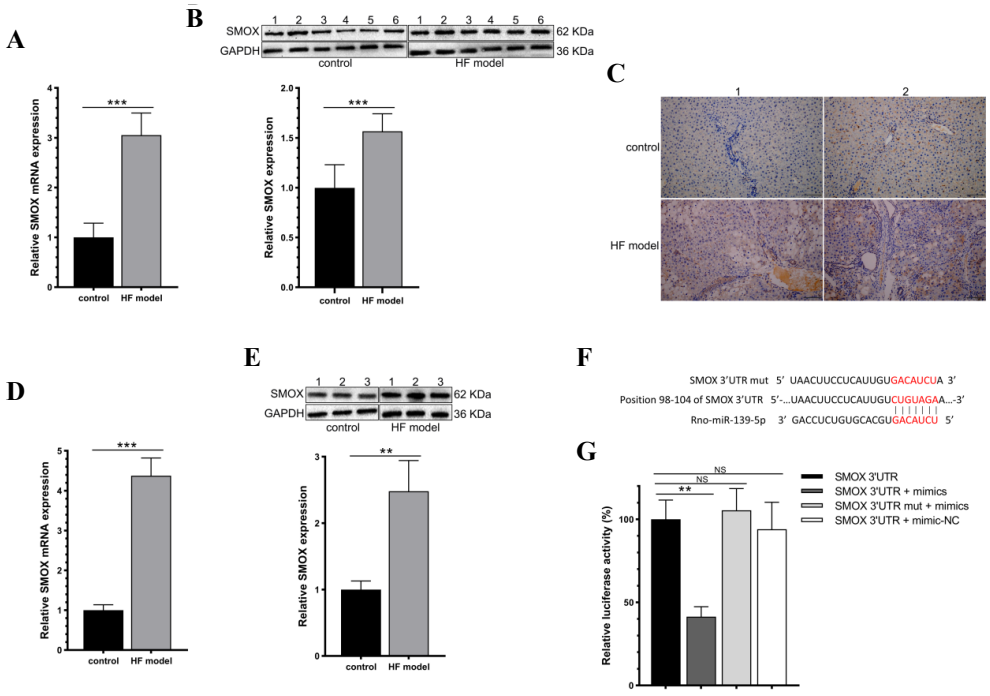

Figure 2. Expression level of SMOX in HF models and the targeting relationship between miR-139-5p and SMOX

Notes: (A) SMOX mRNA expression in rats HF model; (B) SMOX protein expression in rats HF model; (C) SMOX immunohistochemical staining of rats HF model; (D) SMOX mRNA expression in cellular HF model; (E) SMOX protein expression in cellular HF model; (F) Target prediction by Targetscan 7.1; (G) Dual luciferase reporter assay between miR-139-5p and SMOX. **: $P < 0.01$; *** $P < 0.001$.

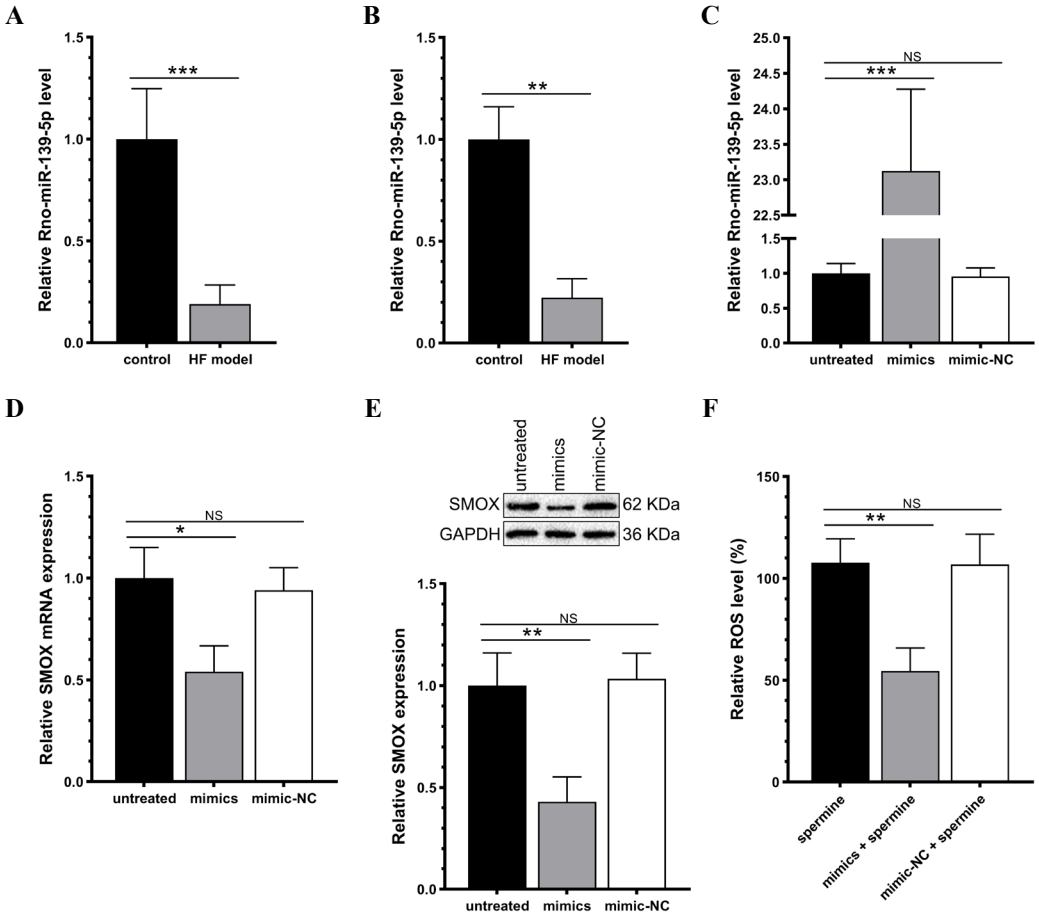

Figure 3. Expression level of Rno-miR-139-5p in HF models and the regulation of miR-139-5p on SMOX

Notes: (A) Rno-miR-139-5p expression in rats HF model; (B) Rno-miR-139-5p expression in cellular HF model; (C) Transfection efficiency of Rno-miR-139-5p mimics and its NC; (D) Relative SMOX mRNA level in cellular HF model transfected Rno-miR-139-5p; (E) Relative SMOX protein level in cellular HF model transfected Rno-miR-139-5p; (F) SMOX enzyme activity of HF cellular model transfected with Rno-miR-139-5p. *: $P < 0.05$; **: $P < 0.01$; *** $P < 0.001$.

4. MiR-139-5p effectively reverses the activation progression of HSC-T6 cells

HSC-T6 cells were transfected with miR-139-5p mimics, miR-139-5p inhibitor, or NC, followed by LPS induction. Transfection efficacy was examined by RT-qPCR (Figure 4A). Interestingly, overexpression of miR-139-5p significantly suppressed the viability of HSC-T6 cells, and knockdown of miR-139-5p enhanced their viability (Figure 4B). The ROS level was downregulated by miR-139-5p mimics and upregulated by miR-139-5p inhibitor (Figure 4C). Transfection with miR-139-5p mimics significantly downregulated mRNA and protein levels of SMOX, α-SMA and TGF-β, and their expression levels were upregulated by knockdown of miR-139-5p (Figure 4D, 4E). It is suggested that miR-139-5p can effectively decreased the activation of HSC-T6 cells.

5. Overexpression of SMOX effectively reverses the ability of miR-139-5p to inhibit the activation of HSC-T6 cells

To investigate the involvement of SMOX in HF progression, we co-intervened SMOX by lentivirus transfection and then miR-139-5p by plasmid transfection. The mRNA level of SMOX was examined to determine the co-transfection efficacy (Figure 5A). Interestingly, overexpression of SMOX enhanced cell viability (Figure 5B), enhanced ROS levels (Figure 5C), and upregulated mRNA and protein levels of α-SMA and TGF-β in HSC-T6 cells (Figure 5D, 5E). More importantly, the regulatory effects of miR-139-5p on HSC-T6 cells were reversed by overexpression of SMOX. Therefore, we confirmed that overexpression of SMOX reversed the inhibitory effect of miR-139-5p on LPS-induced activation of HSC-T6 cells by enhancing ROS levels and promoting cell activation.

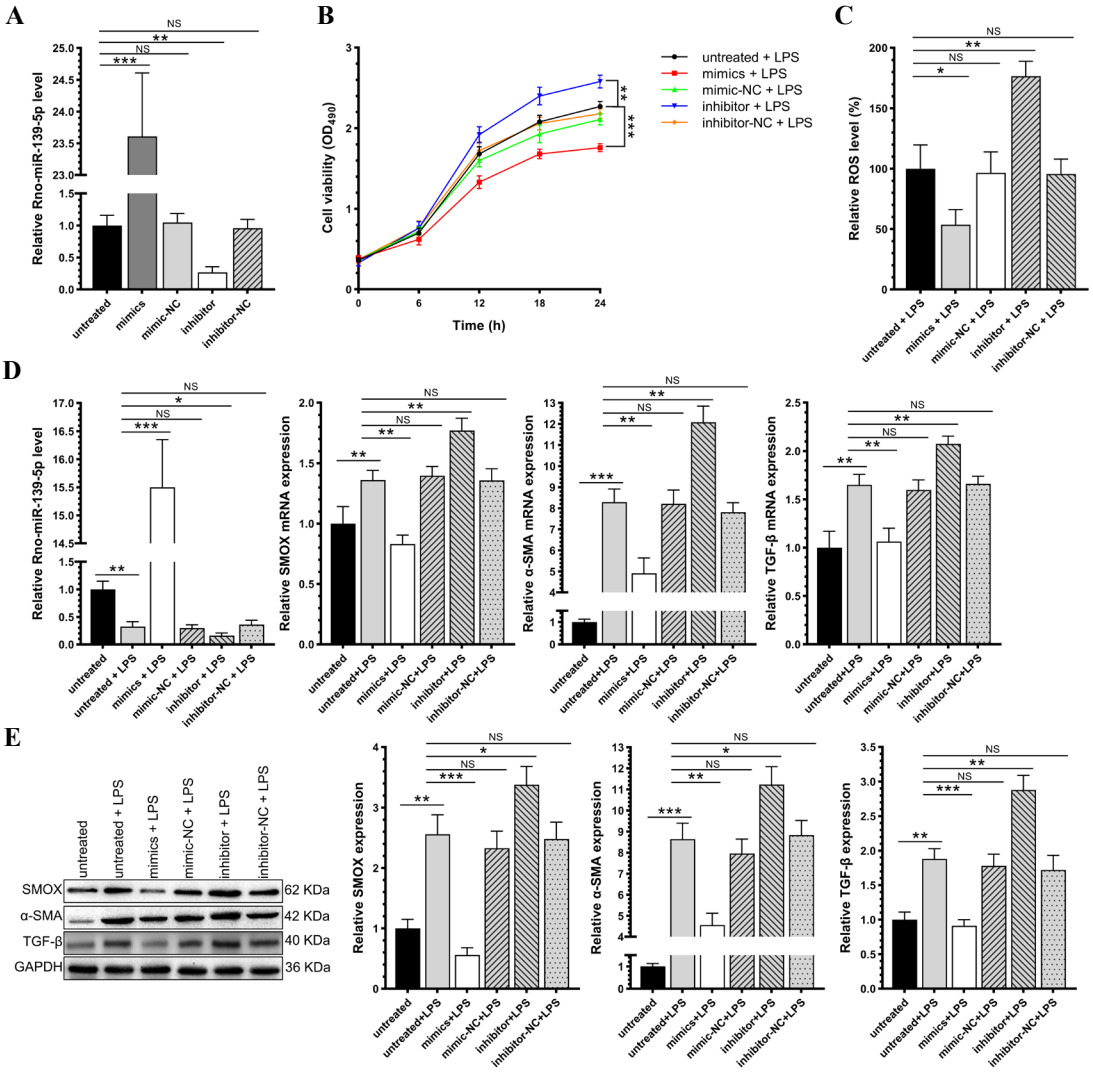

Figure 4. Rno-miR-139-5p effectively reverses the activation progression of HSC-T6 cells

Notes: (A) Transfection efficiency of Rno-miR-139-5p mimics, inhibitor and their NC; (B) Cell viability of HSC-T6 HF model transfected with rno-miR-139-5p mimics, inhibitor and their NC; (C) ROS level of HSC-T6 HF model transfected with rno-miR-139-5p mimics, inhibitor and their NC; (D) Rno-miR-139-5p, SMOX mRNA, α-SMA mRNA and TGF-β mRNA level in HSC-T6 HF model transfected with rno-miR-139-5p mimics, inhibitor and their NC; (E) SMOX, α-SMA and TGF-β expression in HSC-T6 HF model transfected with rno-miR-139-5p mimics, inhibitor and their NC. *: $P < 0.05$; **: $P < 0.01$; *** $P < 0.001$.

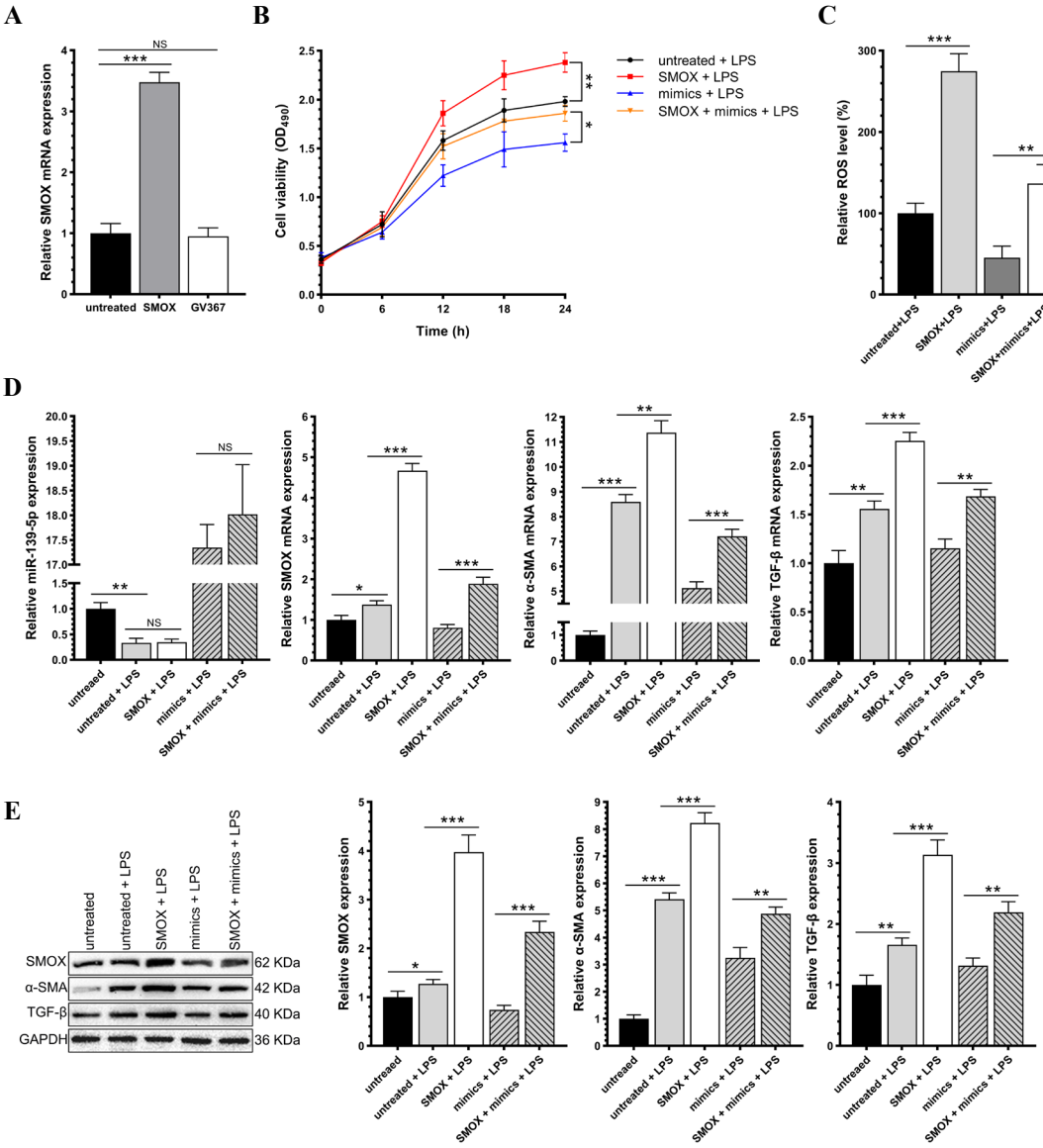

Figure 5. Overexpression of SMOX effectively reverses the ability of miR-139-5p to inhibit the activation of HSC-T6 cells

Notes: (A) Lentivirus infection efficiency of SMOX overexpression; (B) Cell viability of HSC-T6 HF model transfected with SMOX or rno-miR-139-5p; (C) ROS level of HSC-T6 HF model transfected with SMOX or rno-miR-139-5p; (D) Rno-miR-139-5p, SMOX mRNA, α-SMA mRNA and TGF-β mRNA level in HSC-T6 HF model transfected with SMOX or rno-miR-139-5p; (E) SMOX, α-SMA and TGF-β expression in HSC-T6 HF model transfected with SMOX or rno-miR-139-5p; *: $P < 0.05$; **: $P < 0.01$; *** $P < 0.001$.

Discussion

As an important link in chronic liver diseases, HF is the main cause of the onset and death of patients with chronic viral hepatitis or obesity-related fatty liver disease. Without active interventions, HF ultimately leads to liver cirrhosis and hepatocellular carcinoma (Hernandez-Gea & Friedman, 2011; Lim & Kim, 2008). HF is a complex and dynamic process involving various types of cells (Lee, Wallace, & Friedman, 2015), but the specific pathogenesis has not yet been fully elucidated. Inflammatory response and oxidative stress are the key factors driving the development of HF (Nielsen et al., 2019). During the progression of HF, abundant ROS are produced by damaged parenchymal liver cells. This directly activates the redox-sensitive signaling pathways in HSCs, which then results in the activation of HSCs and positive expression of ECM (Brenner et al., 2011). With the increased incidence in liver cirrhosis and the huge economic burden, it is a challenging task to reverse and alleviate HF by monitoring potential biomarkers.

The tumor-related roles of miRNAs have been extensively explored, and a growing number of studies has shown the vital functions of miRNAs in mediating signaling pathways responsible for activating HSCs (Jiang, Ai, Wan, Zhang, & Wu, 2017). Men et al. (Men et al., 2017) showed that miR-145 is upregulated in primary rat HSCs and TGF-β-induced activated HSCs in vitro, and it stimulates HSC activation and HF by

targeting KLF4. Wang et al. (Wang et al., 2021) found that a deficiency in miR-223 accelerates HF induced by chronic CCl_4 induction. Overexpression of miR-223 downregulates Gli2 and PDGFRA/B, thus suppressing the activation and proliferation of HSCs. MiR-223 inhibits HF by targeting multiple genes in hepatocytes and HSCs, thus providing a potential therapeutic target for HF. He et al. (He, Shu, Zhou, Zhang, & Yang, 2021) proved that miR-139-5p blocks TGF-β-induced activation of HSCs by targeting PMP22.

miR-139-5p was recently discovered and analyzed for its biological functions. Wu et al. (Wu, Zhang, Chen, & Ha, 2020) reported that the expression level of miR-139-5p decreased significantly in hepatocellular carcinoma, directly targeted SLITRK4, and affected the proliferation and invasion of hepatocellular carcinoma cells through miR-139-5p/SLITRK4. The research of Wei et al. (Wei et al., 2020) confirmed that up-regulation of miR-139-5p protects diabetic mice from liver tissue damage and oxidative stress through inhibiting Notch signaling pathwaypathway in HCC growth and progression and may provide new targets for us to better arrange the progression of HCC. Through literature review, it was determined that the role of miR-139-5p in the development of HF has been rarely reported. He et al. (He et al., 2021) reported that miR-139-5p targets the 3'UTR of PMP22 and inhibits PMP22 expression; miR-139-5p hinders TGF-β-induced HSCs activation through targeting PMP22 and modulates TGF-β-induced hepatic stellate cell activation and CCl 4-induced hepatic fibrosis in mice.Here, we first established an in vivo HF model through subcutaneously injecting CCl_4 in rats. Downregulated miR-139-5p and upregulated α-SMA and TGF-β were observed in the liver tissues of HF rats compared with those of the controls. In LPS-induced HSC-T6 cells, miR-139-5p was significantly downregulated. Overexpression of miR-139-5p markedly inhibited the viability of activated HSC-T6 cells, and downregulated mRNA and protein levels of α-SMA and TGF-β. As expected, the opposite results were obtained after knockdown of miR-139-5p. The activation of HSCs was reflected by the viability and expression levels of α-SMA and TGF-β, respectively. Therefore, miR-139-5p effectively alleviated the activation of HSC-T6 cells and the progression of HF.

SMOX is a member of the polyamine oxidase family. It produces a large amount of hydrogen peroxide in the cytoplasm and nucleus, and it is an ROS precursor, and thus causes DNA damage repair, inflammatory response, and is involved in cancer-related signaling pathways (Murray-Stewart et al., 2016). Sierra et al. (Sierra et al., 2020) found that SMOX-deficient mice have a significantly reduced spermidine level in the stomach and decreased inflammation induced by Helicobacter pylori. In addition, treatment of the SMOX inhibitor in human gastric organs indicated that SMOX is correlated with the activation of β-catenin, and suggests that SMOX promotes H. pylori-induced carcinogenesis of gastric cancer by causing inflammation, DNA damage, and activation of β-catenin signaling.

Zhang et al. (Zhang et al., 2019) reconstructed a general genome-scale metabolic model of colorectal cancer (CRC), which revealed that SMOX is the key factor that alters the metabolism in the microenvironment of CRC. Fratini et al. (Fratini et al., 2019) reported that overexpression of SMOX induces cell stress through imbalanced ROS production in neuroblastoma (NB) cells and a SMOX transgenic mouse model. They also confirmed that upregulation of the apoptosis antagonistic transcription factor (AATF) is driven by overexpressed SMOX in NB cells and total-SMOX mice, indicating that SMOX serves as a novel anti-apoptotic marker in NB cells. Hu et al. (Hu et al., 2018) proposed that SMOX is overexpressed in hepatocellular carcinoma (HCC) cell lines and clinical specimens of HCC, and promotes the proliferation of HCC cells by regulating the PI3K/AKT signaling pathway.

Consistently, our findings showed that SMOX was upregulated in rat fibrotic liver tissues, and was also upregulated in activated HSC-T6 cells. This indicated that SMOX could be involved in the progression of HF. As predicted by Targetscan 7.2, miR-139-5p may bind with the SMOX 3'-UTR. Transfection of miR-139-5p mimics downregulated mRNA and protein levels of SMOX, and reduced the ability to degrade spermine in HSC-T6 cells. Knockdown of miR-139-5p yielded the opposite results. It is suggested that miR-139-5p directly targets SMOX, and reduced its mRNA and protein levels as well as activity. In addition, overexpression of SMOX in HSC-T6 cells significantly enhanced ROS levels and the activation of HSC-T6 cells. More importantly, overexpression of SMOX reversed the inhibitory effect of miR-139-5p on LPS-induced activation of HSC-T6 cells.

Conclusion

MiR-139-5p is significantly downregulated in the progression of HF, which slows the progression of HF by targeting and downregulating SMOX. Thus, miR-139-5p can serve as a potential biomarker and therapeutic target of HF.

Declaration

The authors declared that they have no conflicts of interest to this work.

The authors declared that data and material in the manuscript are available.

Funding

This project was funded by the Jiangxi Provincial Outstanding Talent Fund (grant no. 20192bcb23022), the National Natural Science Foundation of China (grant no. 81960121), and the Natural Science Foundation of Jiangxi Province (grant no. 20202BAB206008).

References

[1] Brenner DA, Seki E, Taura K, Kisseleva T, Deminicis S, Iwaisako K., Inokuchi S, Schnabl B; Oesterreicher CH, Paik YH, Miura K, Kodama, Y. Non-alcoholic steatohepatitis-induced fibrosis: Toll-like receptors, reactive oxygen species and Jun N-terminal kinase. Hepatol Res. 2011;41(7):683-86.

[2] Cervelli, M, Amendola, R, Polticelli F, & Mariottini P. (2012). Spermine oxidase: ten years after. Amino Acids. 2012;42(2-3):441-50.

[3] Coulouarn C, Clement B. Stellate cells and the development of liver cancer: therapeutic potential of targeting the stroma. J Hepatol. 2014; 60(6):1306-9.

[4] Fratini E, Cervelli M, Mariottini P, Kanamori Y, Amendola R, Agostinelli E. Link between spermine oxidase and apoptosis antagonizing transcription factor: A new pathway in neuroblastoma. Int J Oncol. 2019;55(5):1149-56.

[5] He C, Shu B, Zhou Y, Zhang R, Yang X. The miR-139-5p/peripheral myelin protein 22 axis modulates TGF-beta-induced hepatic stellate cell activation and CCl4-induced hepatic fibrosis in mice. Life Sci. 2021;276:119294.

[6] Hernandez-Gea V, Friedman SL. Pathogenesis of liver fibrosis. Annu Rev Pathol. 2011;6:425-56.

[7] Hu T, Sun D, Zhang J, Xue R, Janssen HLA, Tang W, Dong L. Spermine oxidase is upregulated and promotes tumor growth in hepatocellular carcinoma. Hepatol Res. 2018;48(12):967-77.

[8] Jesudian A, Desale S, Julia J, Landry E, Maxwell C, Kallakury B, Laurin J, Shetty, K. Donor Factors Including Donor Risk Index Predict Fibrosis Progression, Allograft Loss, and Patient Survival following Liver Transplantation for Hepatitis C Virus. J Clin Exp Hepatol. 2016;6(2):109-14.

[9] Jiang XP, Ai WB, Wan LY., Zhang YQ, Wu JF. The roles of microRNA families in hepatic fibrosis. Cell Biosci. 2017;7,34.

[10] Jie M, Feng T, Huang W, Zhang M, Feng Y, Jiang H, Wen Z. (2021). Subcellular Localization of miRNAs and Implications in Cellular Homeostasis. Genes (Basel). 2021;12(6)856.

[11] Lee YA, Wallace MC, Friedman SL. (2015). Pathobiology of liver fibrosis: a translational success story. Gut.2015;64(5), 830-41.

[12] Leonetti A, Cervoni L, Polticelli F, Kanamori Y, Yurtsever ZN, Agostinelli E, Mariottini P, Stano P, Cervelli M. Spectroscopic and calorimetric characterization of spermine oxidase and its association forms. Biochem J;2017. 474(24), 4253-68.

[13] Lim YS, Kim WR. The global impact of hepatic fibrosis and end-stage liver disease. Clin Liver Dis. 2008;12(4):733-46, vii.

[14] Men R, Wen M, Zhao M, Dan X, Yang Z, Wu W, Wang MH, Liu X, Yang L. MircoRNA-145 promotes activation of hepatic stellate cells via targeting kruppel-like factor 4. Sci Rep. 2017;7:40468.

[15] Murray-Stewart T, Sierra JC, Piazuelo MB, Mera RM, Chaturvedi R, Bravo LE, Correa P, Schneider BG, Wilson KT, Casero RA. Epigenetic silencing of miR-124 prevents spermine oxidase regulation: implications for Helicobacter pylori-induced gastric cancer. Oncogene. 2016;35(42):5480-88.

[16] Nielsen J, Christensen VB, Borgwardt L, Rasmussen A, Østrup O, Kjær MS. Prognostic molecular markers in pediatric liver disease - Are there any? Biochim Biophys Acta Mol Basis Dis. 2019;1865(3):577-86.

[17] Sierra JC, Piazuelo MB, Luis PB, Barry DP, Allaman MM, Asim M, Sebrell TA, Finley JL, Rose KL, Hill S, Holshouser SL, Casero RA, Cleveland JL, Woster PM, Schey KL, Bimczok D, Schneider C, Gobert AP, Wilson KT. Spermine oxidase mediates Helicobacter pylori-induced gastric inflammation, DNA damage, and carcinogenic signaling. Oncogene. 2020;39(22):4465-74.

[18] Suzuki HI, Katsura A, Matsuyama H, Miyazono K. MicroRNA regulons in tumor microenvironment. Oncogene. 2015;34(24):3085-94.

[19] Tsai MK, Lin YL, Huang YT. Effects of salvianolic acids on oxidative stress and hepatic fibrosis in rats. Toxicol Appl Pharmacol. 2010;242(2):155-64.

[20] Wang X, Seo W, Park SH, Fu Y, Hwang S, Rodrigues RM, Feng D, Gao B, He Y. MicroRNA-223 restricts liver fibrosis by inhibiting the TAZ-IHH-GLI2 and PDGF signaling pathways via the crosstalk of multiple liver cell types. Int J Biol Sci. 2021;17(4):1153-67.

[21] Wei H, Huang L, Wei F, Li G, Huang B, Li J, Cao C. Up-regulation of miR-139-5p protects diabetic mice from liver tissue damage and oxidative stress through inhibiting Notch signaling pathway. Acta Biochim Biophys Sin (Shanghai). 2020;52(4):390-400.

[22] Wu J, Zhang T, Chen Y, Ha S. MiR-139-5p influences hepatocellular carcinoma cell invasion and proliferation capacities via decreasing SLITRK4 expression. Biosci Rep. 2020;40(5):BSR20193295.

[23] Xiao J, Wang F, Wong NK, He J, Zhang R, Sun R, Xu Y, Liu Y, Li W, Koike K, He W, You H, Miao Y, Liu X, Meng M, Gao B, Wang H, Li C. Global liver disease burdens and research trends: Analysis from a Chinese perspective. J Hepatol. 2019;71(1):212-21.

[24] Zhang C, Aldrees M, Arif M, Li X, Mardinoglu A, Aziz MA. Elucidating the Reprograming of Colorectal Cancer Metabolism Using Genome-Scale Metabolic Modeling. Front Oncol. 2019;9:681.